Wireless Three-pad ECG System: Challenges, Design and Evaluations

Huasong Cao, Haoming Li, Leo Stocco, and Victor C.M. Leung

***Abstract*—Electrocardiography (ECG) is a widely accepted approach for monitoring of cardiac activity and clinical diagnosis of heart diseases. Since cardiologists have been well-trained to accept 12-lead ECG information, a huge number of ECG systems are using such number of electrodes and placement configuration to facilitate fast interpretation. Our goal is to design a wireless ECG system which renders conventional 12-lead ECG information. We propose the three-pad ECG system (W3ECG). W3ECG furthers the pad design idea of the single-pad approach. Signals obtained from these three pads, plus their placement information, make it possible to synthesize conventional 12-lead ECG signals. We provide one example of pad placement and evaluate its performance by examining ECG data of four patients available from online database. Feasibility test of our selected pad placement positions show comparable results with respect to the EASI lead system. Experimental results also exhibit high correlations between synthesized and directly observed 12-lead signals (9 out of 12 cross-correlation coefficients higher than 0.75).**

I. Introduction

Electrocardiography (ECG) is a widely accepted approach for ambulatory monitoring of cardiac activity and clinical diagnosis of heart diseases [1]. By measuring body-surface potentials at a number of electrodes, an ECG system presents time series of potential differences across these electrode placement locations. **This electrical signal is periodic in time (reflecting a cardiac cycle), and each period can be divided into segments for easy identification (e.g., P-R interval, QRS complex and S-T interval) [2]. The tracing of a body-surface potential difference between two electrodes (or between an electrode and a composite of electrical signals from a combination of other electrodes) is referred to as a lead.**

There is no consensus on either the optimal quantity or placement positions of an ECG system's electrodes [3]; they largely depend on which part of a heart is under scrutiny and what a caregiver tries to identify (e.g., levels of dissolved salts or damages to the conductive tissues). While the two parameters are yet to be optimized, various ECG systems have been developed. They can be classified into four groups, namely conventional 12-lead ECG systems, electrocardiographic body surface mapping (BSM) systems, vectorcardiographic (VCG) systems, and wireless ECG systems. Each system can be seen as a particular configuration of the above two parameters.

This work was supported in part by the Canadian Natural Sciences and Engineering Research Council under grant STPGP 365208-08. It is an expanded version of a regular paper and a demo paper presented at Bodynets 2010, Corfu, Greece. The authors are with the Department of Electrical and Computer Engineering, The University of British Columbia, Vancouver, BC, Canada V6T 1Z4; emails {huasongc, hlih, leos, vleung}@ece.ubc.ca. Please address all correspondence to Mr. Huasong Cao at the above email address.

Conventional 12-lead ECG systems require placement of **9 electrodes on pre-defined locations of a subject (yellow and green dots in Fig. 1). These 9 electrodes plus a ground electrode form 12 leads, and are conventionally named leads I, II, III, aVR, aVL, aVF, V1, V2, V3, V4, V5 and V6.** Since cardiologists have been well-trained to accept 12-lead ECG information, a huge number of ECG systems are using such number of electrodes and placement configuration to facilitate fast interpretation [4].

In BSM systems, a large number of electrodes (32 to 219) are placed on strips which are arranged around the circumference of a subject's torso. The potentials are illustrated on a map of body surface model **(e.g., Dalhousie's model shown in Fig. 1), which provides caregivers/researchers knowledge of bio-potential distribution on the torso** [5][6][7]. However, the deployment complexity of BSM systems hinders their wide employment in the clinical environment.

A VCG system [8] registers electrical heart activity in three orthogonal leads. Based on a hypothesis that the heart activity can be modelled by a stationary dipole [9], signals recorded by a VCG system can be transformed to the 12-lead format. The advantage of this approach is the reduced number of electrodes. However, mobility of the subject is still limited.

In order to make ECG sensing units portable, easy to setup, comfortable to patients and tolerant of artifacts, endeavours have been made to design wireless single-pad ECG systems [10][11][12]. The so-called single-pad is a self-contained printed circuit board (PCB) with a front-end amplification circuit, a micro-controller unit, a radio chip and (disposable) electrodes. Body-surface potential differences registered at the unit is wirelessly transmitted to a personal server for storage or analysis. However, as an ECG signal is lead placement dependent, using one single-pad sensing unit, it is impossible to render caregivers conventional 12-lead ECG waveforms.

To tackle the problem, we propose the wireless three-pad ECG system (W3ECG). We apply the linear transformation method of VCG systems to ECG signals registered at three portable sensing units (pads), so as to synthesize conventional 12-lead ECG waveforms.

The rest of this paper is organized as follows. Section II walks the readers through the derivation of the transformation equations used to synthesize 12-lead waveforms. Section III discusses the system design challenges and solutions. Section IV describes current W3ECG implementation. Section V presents practical evaluation results. Section VI concludes the paper and discusses future work.

II. Derivation of Transformation Equations

We first review the heart-vector projection theory [13]. Then by analyzing the clinical data sets available from Dalhousie University, we derive equations for linear transformation from W3ECG signals (obtained from the three W3ECG pads) to the 12-lead format.

A. Heart-vector Projection Theory

It is widely accepted that the electrical heart activity can be modelled as a stationary dipole [14][8]. Under this assumption, the heart dipole moment is a function of time and represented by a vector in the three-dimensional space as

$$\overline{p} = p_x\overline{x} + p_y\overline{y} + p_z\overline{z} \tag{1}$$

where x, y and z are standard unit vectors of a rectangular coordinate system. x and y axes span the frontal plane, x and z axes span the transverse plane, and y and z axes span the sagittal plane. In (1), p_x, p_y and p_z are projections of the heart dipole moment $\overline{p}$ on three axes, representing the scalar components of $\overline{p}$. This is illustrated in Figure 2. Elements of $\overline{p}$ are in units of $mA \times cm$.

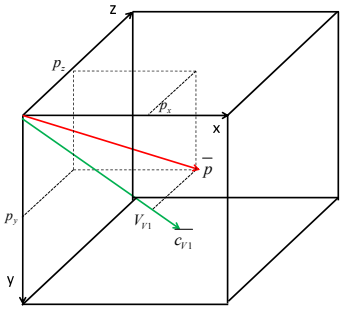

Fig. 2. Illustration of the heart vector and its projection on a lead vector.

The potential V_i (subscript i is for distinguishing torso locations) $\overline{p}$ produces on the torso is the multiplication of $\overline{p}$ and a resistive component $\overline{c_i}$, which is a function of shape, size, and characteristics of the medium, the position of the dipole as well as where the potential is measured (position of electrode on torso). Assuming homogeneity and thus linearity of the medium, the electric potential appearing at any torso location is represented as the projection of $\overline{p}$ on $\overline{c_i}$ as

$$V_i = \overline{c_i} \cdot \overline{p} \tag{2}$$

where $\overline{c_i}$ is called the lead vector with units of Ω/cm. For example, as shown in Figure 2, the lead V1 in the 12-lead system can be expressed as

$$V_{V1} = \overline{c_{V1}} \cdot \overline{p} \tag{3}$$

B. Clinical Data

Two sets of data [9][15] are obtained from Dalhousie University. The first set includes 352 lead vectors for 352 nodes on the human torso derived from computer simulations. The second set includes coefficients for predicting the 352 nodes from EASI leads obtained through practical experiments and interpolations (EASI lead system is an example of VCG system variant, which has been approved by the US Food and Drug Administration for assessing normal, abnormal, and paced cardiac rhythms and for detecting myocardial ischemia or silent ischemia [15]. **EASI lead system gets its name from the electrode placement locations identified as E, A, S and I (red dots in Fig. 1). Leads ES, AS and AI thus refer to tracing of potential differences of corresponding locations). Essentially, these two sets of data are representations of same leads in two coordinate systems: one is the heart dipole rectangular coordinate system; the other is the non-rectangular coordinate system spanned by leads ES, AS and AI. This data is used to derive the equation for transformation.**

C. Derivation Based on Lead Vectors

If the lead vectors for three pads are $\overline{c_A}$, $\overline{c_B}$ and $\overline{c_C}$, according to (2), the potentials measured at the pads can be represented as:

$$V_A = \overline{c_A} \cdot \overline{p} \tag{4}$$

$$V_B = \overline{c_B} \cdot \overline{p} \tag{5}$$

$$V_C = \overline{c_C} \cdot \overline{p} \tag{6}$$

Combining the three measured potentials into a vector $\overline{V_3}$, and three lead vectors into a 3×3 lead matrix $\overline{\overline{c_3}}$, we have (7). This is illustrated in Figure 3.

$$\overline{V_3} = \overline{\overline{c_3}}\,\overline{p} \tag{7}$$

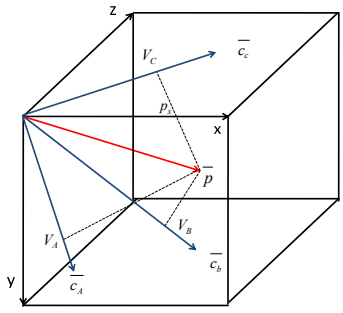

Fig. 3. Illustration of the heart vector and three lead vectors.

When the three lead vectors are linearly independent, the heart vector can be computed as

$$\overline{p} = \overline{\overline{c_3^{-1}}}\,\overline{V_3} \tag{8}$$

The heart vector moment $\overline{p}$ can be computed from the three lead vectors if and only if $\overline{\overline{c_3^{-1}}}$ exists and is obtainable. It is not possible to fully represent cardiac activity by any single lead. At least three are necessary.

Once the heart vector moment is known, the 12-lead standard potentials can be computed by projecting $\overline{p}$ onto the corresponding 12-lead vectors. Take lead $V1$ for example. Combining (3) and (8), lead $V1$ can be computed as:

$$\overline{V_{V1}} = \overline{c_{V1}}\,\overline{\overline{c_3^{-1}}}\,\overline{V_3} \tag{9}$$

The same approach can be used to compute the other eleven leads in the conventional 12-lead system, which can be expressed in vector format as in (10), where each row in $\overline{\overline{c_{12}}}$ is a lead vector of the 12-lead system, and the same row in $\overline{V_{12}}$ is the electric potential measured.

$$\overline{V_{12}} = \overline{\overline{c_{12}}}\,\overline{\overline{c_3^{-1}}}\,\overline{V_3} \tag{10}$$

We rewrite (10) as

$$\overline{V_{12}} = \overline{\overline{T}}\,\overline{V_3} \tag{11}$$

We define $\overline{\overline{T}}$ in (11) as the transformation matrix, representing the transformation coefficients between two vectors, $\overline{V_3}$ and $\overline{V_{12}}$. The lead vectors needed for the matrix $\overline{\overline{c_{12}}}$ in (10) are directly available in the computer-simulation-based data set as mentioned above. The lead vectors for the three pads to compute $\overline{\overline{c_3^{-1}}}$ in **(10)** are calculated by substracting two corresponding lead vectors, each of which is one node in the same data set.

Equation (10) provides a method of generating standard 12-lead ECG signals from 3-lead ECG signals. Specifically, if three electric potential traces are recorded at the three leads, traces for all 12-lead ECG can be synthesized.

D. Derivation Based on Coefficients from EASI Leads

Similar to (11), for an EASI lead system, we can obtain (12), where $\overline{\overline{U_{12}}}$ is equivalent to $\overline{\overline{T}}$ in (11), representing transformation coefficients from EASI leads to the 12 leads.

$$\overline{V_{12}} = \overline{\overline{U_{12}}}\,\overline{V_{EASI}} \tag{12}$$

Equation (12) can be extended to express the transformation from EASI leads to our three-pad leads as follows

$$\overline{V_3} = \overline{\overline{U_3}}\,\overline{V_{EASI}} \tag{13}$$

Combining (12) and (13), results in:

$$\overline{V_{12}} = \overline{\overline{U_{12}}}\,\overline{\overline{U_3^{-1}}}\,\overline{V_3} \tag{14}$$

Equation (14) is in the same expression as (10), but with different notations. The transformation matrices $\overline{\overline{U_{12}}}$ and $\overline{\overline{U_3^{-1}}}$ in (14) are counterparts of $\overline{\overline{c_{12}}}$ and $\overline{\overline{c_3^{-1}}}$ in (10) respectively. In essence, $\overline{\overline{U_{12}}}$ and $\overline{\overline{U_3^{-1}}}$ represent the corresponding transformation coefficients in the coordinate system spanned by EASI leads.

III. Wireless Three-pad ECG System

Our goal is to design a wireless ECG system which renders conventional 12-lead ECG information. Here, wireless refers to not only the data link between a subject and a peripheral monitoring/storage device, but also the connections between sensing units placed on the subject. According to above discussion and derivation, it is theoretically possible to transform ECG signals registered at three sensing units to 12-lead format as long as these three signals come from linearly independent leads. In practice, however, there are a number of challenges need to be addressed to guarantee reliable transmission and accurate transformation.

A. Network Topology and Data Reliability

Three wireless pads and a possible monitoring/stroage device make our W3ECG a wireless body area sensor network (WBASN) [16]. Among existing standards, IEEE 802.15.4 [17] stands out for its low power consumption and simplicity. However, previous study [18] has showed that in a contention-based wireless access network, system performance (packet reception ratio) degrades severely when more than two sensor devices transmitting in a relatively high data rate, even for a single hop. Our study [19] also showed that a ZigBee network performs intolerable **in terms of** packet reception ratio and fairness, when the number of hops is increased. These suggest our selection of a contention-free and single-hop wireless network when data reliability is crucial. Fortunately, these two properties are supported in the IEEE 802.15.4 standard.

Two operation modes are **supported in IEEE 802.15.4**, namely beacon-enabled mode and non-beacon-enabled mode. Beacon-enabled mode utilizes a slotted-CSMA (carrier sense multiple access) approach in contention access period (CAP) and a time division multiple access (TDMA) approach in contention-free period (CFP). Figure 4 illustrates the superframe structure in the beacon-enabled mode. It consists of two portions: an active and an inactive portions. The active part is equally divided into *aNumbSuperframeSlots* slots, which are then grouped into beacon, CFP and CAP.

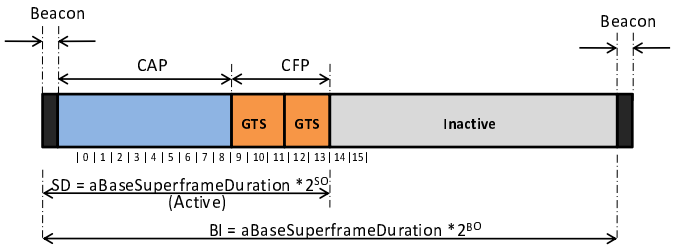

Fig. 4. Superframe structure of IEEE 802.15.4 beacon-enabled mode.

The length of a superframe and its active part, given by the beacon interval (BI) and superframe duration (SD), are defined as

$$BI = aBaseSuperframeDuration \times 2^{BO} \tag{15}$$

$$SD = aBaseSuperframeDuration \times 2^{SO} \quad (16)$$

where BO is the beacon order, and SO is the superframe. These two parameters are determined and communicated by the network coordinator of the network through beacons delimiting the superframes.

Based on protocols of the beacon-enabled mode, we have proposed a quality-of-service (QoS) provisioning framework [20] to facilitate WBASN applications including W3ECG. As a result, the W3ECG network is organized in a star topology. A personal server acts as a network coordinator and coordinates data communications of the three pads (end-devices in the IEEE 802.15.4 network). Data can be stored locally at the personal server, forwarded to caregivers' database, or synthesized for real-time analysis.

The favor of the superframe approach over a TDMA mechanism [21], is due to extensibility considerations. Firstly, the CAP can be utilized to accommodate traffic generated by sensors with bursty data, e.g., alarm and control signals. Secondly, allocation of time slots are dynamically updated in runtime to allow admissions of new sensors with periodic data. However, it imposes higher requirements on both oscillator accuracy and software efficiency [22][23] during implementation.

Our simulation study in [20] showed that CFP throughput increases with increasing number of admitted traffic, and saturates at roughly 22 Kbps, which is well enough for a W3ECG's three wireless channels. Plus, a high time-constraint compliance ratio (above 99%) for admitted traffic shall satisfy the requirements for clinical usage of W3ECG.

B. Time Synchronization and Data Latency

Two types of synchronization are considered. One is the synchronization of wireless communications of three pads, and the second is the synchronization of sampling processes on these pads. The former one is achieved by conforming to the standard in order to ensure all transceivers work at the same pace, while the latter one's realization is user-specific. However, having data communications synchronized to a superframe structure does offer a solution to initiate sampling processes at three pads simultaneously.

The time delay T_d between a personal server issuing a command and a pad initiating sampling can be expressed as the sum of propagation delay T_{prog} and processing delay T_{proc} (as in (18)).

$$T_d = T_{prog} + T_{proc} \quad (17)$$

Considering all three pads are in close proximity to the personal server, differences between propagation delays are neglectable. Plus, as each pad is uniformly manufactured and programmed, processing delays (caused by transceivers and software event handling) shall be the same. Therefore, if sampling processes at three pads are triggered by a command through a packet from the personal server, they can be synchronized to the same starting point.

A same starting point however does not guarantee perfect synchronization due to drifts of individual oscillators onboard. As a consequence, another command packet need to be broadcasted to re-synchronize sampling processes after a while. So how frequent this re-synchronization takes place? It depends on the oscillator's frequency and parts per million (ppm). For example, assuming a oscillator with 62.5 kHz frequency and 40 $\pm$ppm [24], and also assuming a 250 Hz sampling frequency for ECG signal [25], it takes 25 s to incur a sample delay. If we want to limit this delay to be within 10% of a sample period, a re-synchronization command need to be triggered less than every 2.5 s.

Next to determine is where to insert these two command packets. First of all, the time has to be when all transceivers are on, meaning it can not be the inactive portion of a superframe. Secondly, the transmission shall be contention-free. These both suggest putting the commands along with a beacon frame. Fortunately, adding beacon-frame payload is supported in IEEE 802.15.4 standard.

Further to the discussion of the length of a superframe, it determines the allowable number of superframes a personal server can wait before sending the next re-synchronization packet. Take the 2.5 s interval (calculated above) for example, Table I lists the numbers of superframes between re-synchronization packets with varying BO ($BO = SO$) and corresponding superframe lengths (left three columns).

BO	Superframe Length (ms)	No. of Superframes between Re-sync.	Maximum ECG Data Latency (ms)
0	15.36	162	13
1	30.72	81	23
2	61.44	40	44
3	122.88	20	85
4	245.76	10	167
5	491.52	5	331

TABLE I
NUMBER OF SUPERFRAMES BETWEEN RE-SYNCHRONIZATION PACKETS AND ECG DATA LATENCY VS. BO

Also calculated and listed in the right column of Table I is the maximum latency (rounded up) of accommodated ECG data. Recall this delay is mainly introduced because of the contention-free access in CFP, when time slots are reserved for different pads. Assuming CFP are fully reserved for W3ECG pads, and time slots are equally allocated to them, then the maximum delay $T_d^{'}max$ can be calculated as

$$T_{dmax}^{'} = BI - T_b - (T_{cap})_{min} \quad (18)$$

where T_b and T_{cap} are time of beacon period and CAP (CAP is required to have a minimum length of 440 symbols [17]). Note that BO can be up to 16, however, we deem a delay of ECG data of less than 0.5 s is acceptable for applications asking for real-time analysis.

C. Pad Placement and Data Accuracy

To transform ECG signals registered at three sensing units to 12-lead format, (10) and (14) require that the corresponding leads are linearly independent of each other. Two approaches to ensure this linear independence are discussed below.

1) Two Approaches:

- Suggest one set of placement locations, and instruct the caregiver/patient to place the pads at exactly these locations. The popularity of EASI leads suggest the need to provide locations that can be easily identified in anatomy. In this case, the transformation matrix is unique and precalculated, and linear independence of leads is assured.
- Suggest sets of areas for placement, and instruct the caregiver/patient to place the pads at convenient locations. This approach caters to the needs of surgical operations, female users, or comfort of different individuals. A localization mechanism is needed to determine the pad placement locations during deployment, and to tune the coefficients in the transformation matrix in real-time. The system should give an indication if linear independence of leads is lost.

In the following, we study the first approach only.

2) Suggested Placement Locations: The pad placements are specified in Table II (The numbers in the table refer to node numbers **in Fig. 1), and indicated by the three greyed areas.**

Pad Number	Input A	Input B
Pad 1	109	107
Pad 2	170	127
Pad 3	178	177

TABLE II
SUGGESTED W3ECG PAD PLACEMENTS.

Ideally, each of the three pads is aligned with one axis of the heart vector. However, human organs and skin are not linear resistive components, which makes the alignment to the three axes difficult. The attempt to achieve orthogonality of three vectors leads to the above three placement locations, i.e., pad 1, pad 2 and pad 3 are placed according to the estimated directions of x, y and z in Figure 2.

As a result of the above placements, we obtain $\overline{\overline{U_3}}$, which has a condition number of 2.6069 (EASI lead system has a condition number of 1.0162). It indicates a relatively stable linear transformation. In other words, it is tolerant to placement errors.

3) Feasibility Test: In this section, we evaluate the feasibility of the above pad placement locations. ECG data collected by Dalhousie's BSM system for four patients [26] are examined. Acquired ECG data from these patients are with acute myocardial infarction. Because there were no pads actually placed on these locations, the signals that would appear on the three pads if we were able to place them there are calculated, based on how the differential signal is obtained on each bipolar lead.

We pick recorded potential values for nodes 170 and 127, 178 and 177, as well as 109 and 107 from [26]. Substractions between potential values of the two nodes in each of the pair, for each of the sampling time yield three time series of differential potential values that are then used in (14) to synthesis the simulated 12-lead ECG signals.

We compare the generated 12-lead ECG signals with the directly obtained version by evaluating the cross-correlation coefficients. Assuming the directly obtained signal is $V_i(t)$ (i indicates the 12 different leads), and the synthesized signal is $V_i^{'}(t)$, then the cross-correlation coefficient r_i can be represented as in (19), where $\overline{V_i}$ and $\overline{V_i^{'}}$ are means of $V_i(t)$ and $V_i^{'}(t)$ respectively.

$$r_i = \frac{\sum_t (V_i(t) - \overline{V_i})(V_i^{'}(t) - \overline{V_i^{'}})}{\sqrt{(\sum_t (V_i(t) - \overline{V_i})^2 (\sum_t (V_i^{'}(t) - \overline{V_i^{'}}))^2}} \tag{19}$$

There are 12 coefficients for each patient. In order to prove the effectiveness of W3ECG's approach, these coefficients are shown in Figures 5 to 8 with those obtained by using the EASI approach, for each of the four patients, respectively.

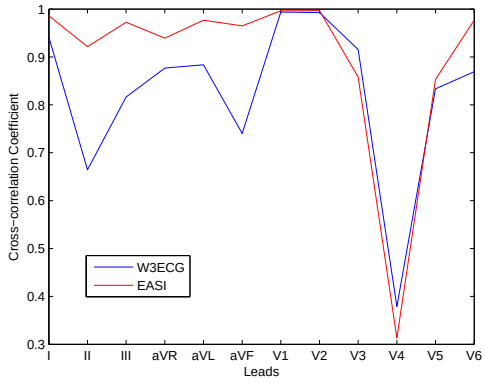

Fig. 5. Comparison of cross-correlation coefficients between W3ECG system and EASI system for Patient 1.

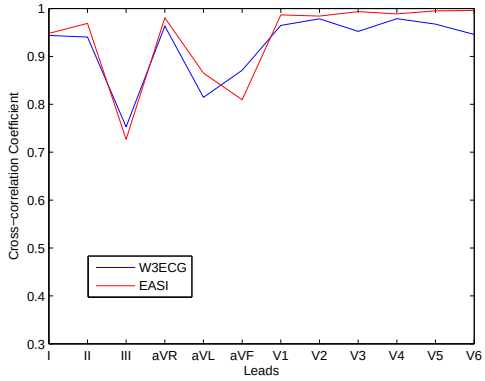

Fig. 6. Comparison of cross-correlation coefficients between W3ECG system and EASI system for Patient 2.

From the above comparisons, we observe a good performance for our proposed W3ECG system for patients 2 and 4, but larger discrepancies for patients 1 (lead V4) and 3 (lead III). This coincides with those of the EASI system. We note for the EASI system, very small coefficients appear (0.3134 for lead V4 of patient 1 and -0.0850 for lead III of patient 3). However, other leads of patients 1 and 3 show high cross correlations in the EASI system. In comparison, having very small coefficients for some leads in the W3ECG system seems

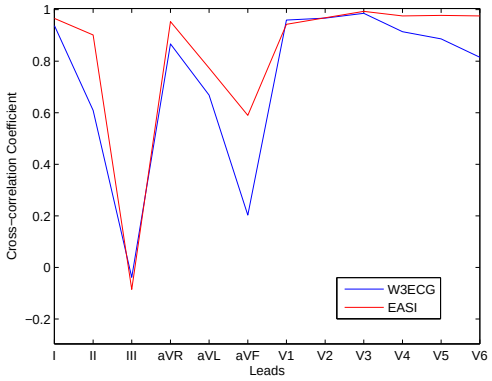

Fig. 7. Comparison of cross-correlation coefficients between W3ECG system and EASI system for Patient 3.

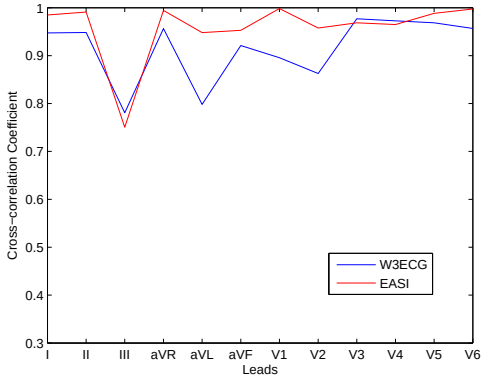

Fig. 8. Comparison of cross-correlation coefficients between W3ECG system and EASI system for Patient 4.

to have a negative effect on the other lead's performance, as we observe that lead II and aVF for patients 1 and 3 also experience small coefficients. This can be explained by the linear dependence our three pads may have on each other.

We also compare the waveforms of the original 12-lead signals and synthesized signals for patient 4 in Figure 9. It gives an idea of how close the waveforms appear for different leads. We note the signals for Lead III for both versions look quite similar in the QRS complex duration, although in Figure 8 we have a relatively smaller cross-correlation coefficient (0.7806). A high degree of similarity between original and generated waveforms also applies to Lead aVL, which has the second least cross-correlation coefficient (0.7983).

IV. Implementations

A. ECG Front-end Circuit

Texas Instruments' instrumentation amplifier INA333 and operational amplifier OPA333 are chosen for our ECG front-end circuit [27]. INA333 is reported to be the industry's lowest power zero-drift instrumentation amplifier. It operates with a 1.8V power supply, a 75uA quiescent current, and a 25uV offset voltage. OPA333 features a power supply of 1.8V and very low offset voltage of 10uV. Together they make it possible to use a coin cell (e.g., CR2032) as the power supply.

Figure 10 is a snapshot of our front-end prototypes. The four items in Figure 10, from left to right, are the circuit's front side, back side, back side with mount buttons, and back side mounted with electrodes, respectively. The upper and lower electrodes are two input electrodes which take in potentials; the middle one is an output electrode, which feeds back AC noise and helps set the body at the appropriate potential. Disposable electrodes are used, which can be easily mounted and unmounted through snap buttons.

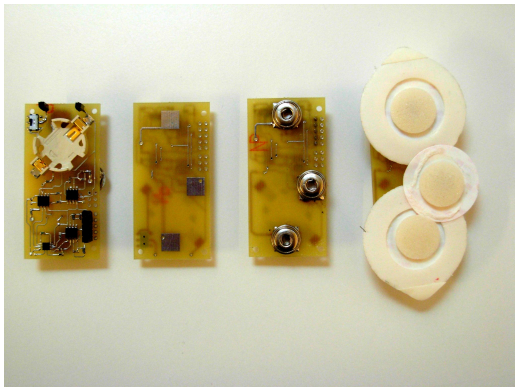

Fig. 10. A snapshot of ECG front-end prototypes.

B. Interface with ***TelosB***

The front-end circuit board is interfaced with an off-the-shelf radio platform, TelosB [28], to enable wireless uploading of registered ECG signal. Figure 11 shows a front and side views of the combined "pad". Since the distance between two input electrodes (refer to the next sub-section) is close to the TelosB's length, our front-end prototype has been made in the same size as a TelosB.

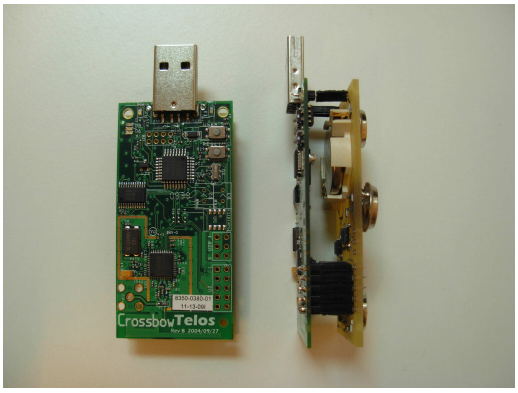

Fig. 11. The front-end circuit interfaced with TelosB.

The coin cell battery that is installed on the front-end circuit supplies power to the TelosB directly. The front-end circuit is in turn supplied by filtered DC voltage from the TelosB.

Amplified ECG signal is fed to an analog-to-digital converter (ADC) port on the TelosB.

C. Standardization of Distance between Two Input Electrodes

Pad placements in W3ECG is based on the Dalhousie's torso model [26][29], in which from neck to waist, numbered transverse levels are 1 inch apart, and positions around transverse sections are supposed to be equiangularly divided. Since the average waistline of an adult is from 37 to 39.7 inches [30], an estimate of the distance between two adjacent nodes in the transverse plane is from 1.15 to 1.24 inches.

On one hand, the smaller a W3ECG pad is (equivalently smaller distance between two input electrodes), the more comfort it offers; on the other hand, the farther away the two input electrodes are, the larger signal-to-noise ratio the pad obtains. The distance has been determined to be two inches, as a good design trade-off that complies with Dalhousie's torso model, and achieves a good signal-to-noise ratio.

D. Software Package

W3ECG's software consists of three parts, which are all based on the TinyOS software platform [31]. Two of the three are nesC codes for manipulating the TelosB (TelosB interfaced with the front-end circuit, and TelosB acting as a gateway), and the other one is Java code running in a server.

1) Sampling and Radio Communications on A Pad: The nesC codes for manipulating pads and the gateway are based on an existing implementation of the IEEE 802.15.4 beacon-enabled mode in TinyOS [23].

2) ADC Configurations: The ADC equipped with MSP430F1611 chip on TelosB provides a 12-bit resolution, and can be configured in four different modes. The single-channel-repeat mode is chosen because only one channel will be continuously used on each pad. The ACLK clock is sourced to ADC to provide a more accurate sampling frequency than SMCLK. The sampling frequency is set to 256 Hz. All the configurations are done through TinyOS interface Msp430Adc12SingleChannel of component Msp430Adc12ClientAutoRVGC(). An event SingleChannel.multipleDataReady() is triggered whenever there are 16 (which is the current maximum allowable value) ADC samples available.

3) Data Buffer Design: A data buffer is created to temporarily store ECG samples before transmission. It is separated from the payload buffer of a TinyOS packet. In other words, ECG samples are firstly moved from this data buffer to the payload buffer, and then forwarded to the radio.

Cyclic array has been chosen as the data structure for the data buffer, and two pointers (write and read) are assigned to provide synchronized access to the buffer. The synchronization is achieved by using the *atomic* keyword for operations involving the two pointers. Each time the event for new ADC samples is triggered, samples are written to the buffer with the write pointer as the offset. As the event is triggered for every 16 samples, the offset specified by either the write or the read pointer is a multiple of 16.

4) Beacon-frame Generation and Data Forwarding on The Gateway: The gateway, known as the PAN coordinator in an IEEE 802.15.4 network, generates a beacon-frame at the beginning of every superframe, and accepts association from each pad (end device in IEEE 802.15.4). We added an implementation to enable serial communications of commands between the gateway and server. Whenever the gateway acknowledges association, a message is created to notify the server of this decision and the corresponding pad ID.

We also implemented the functionality to instruct all pads to synchronize their sampling processes, by adding specific beacon-frame payloads. This is triggered by a command from the server end through a serial connection. Everytime the gateway sends a beacon-frame, it checks whether there is a need to indicate in the payload to start or synchronize the sampling processes on the pads. If so, it sets the corresponding fields and transmits the beacon-frame. As soon as it is done, these fields are reset.

ECG data packets' payloads from each pad are wrapped in TinyOS frames at the gateway, and forwarded to the server over the serial link. No processing on the data is done at the gateway. When wrapping up the payload data, the length, AM type fields in the serial TinyOS frame are set. The AM Type is used to differentiate this packet from the above one for the notification of association.

5) Graphical User Interface and Database on The Server: The server runs a graphical user interface (GUI) based on the TinyOS Oscilloscope implementation. We polished the GUI to display three ECG waveforms in separate graphs as shown in Figure 12, and added tabs to enable switching between 12-lead waveforms.

When the server has been notified by associations from all three pads, it pops up a window and asks if the user wishes to start the system. The system can also be started by clicking the "Start" button, in case the user decides to deploy less than three pads.

The GUI displays a limited duration of ECG waveforms, but stores all samples in a MySQL database. The database currently contains three tables, each of which registers data from one pad. Sampling time and value are registered in each table.

V. Experimental Studies

A. Signal Accuracy

According to suggested pad placement, three pads can be deployed at the positions as shown in Figure 13. Placement positions of electrodes for right arm (RA), left arm (LA) and left leg (LL) are also included as references.

Based on the above W3ECG deployment, synthesized 12-lead ECG waveforms are compared to directly observed 12-lead waveforms, one lead at a time. An additional pad is used to directly register waveform of one of the 12 leads, and compared to the synthesized waveform (synthesized from signals obtained on three W3ECG pads) of the same lead. This setup facilities time synchronization between the two versions of ECG waveforms, and also enables cross-correlation analysis. However, wires which is subject to AC interference,

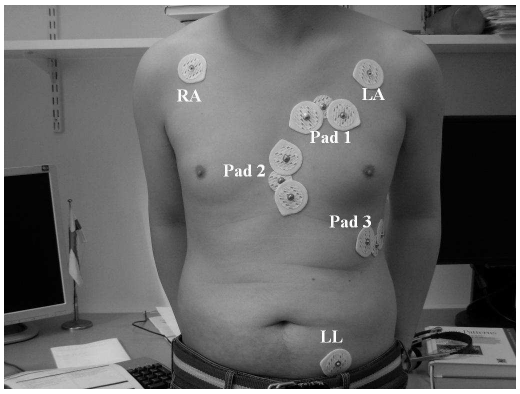

Fig. 13. Placement positions of electrodes for RA, LA and LL, and three sets of electrodes for W3ECG system.

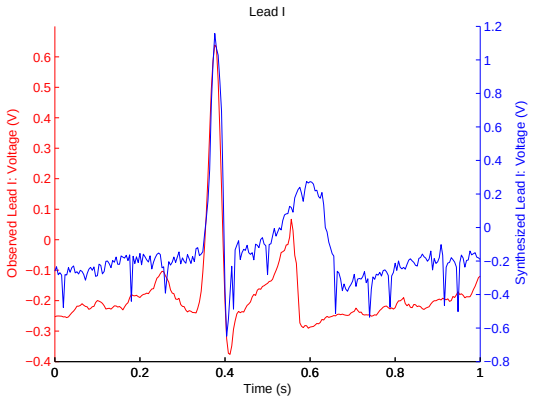

Fig. 14. Comparison between observed and synthesized Lead I signals.

are used to connect electrodes placed on the torso according to conventional 12-lead placements.

Figures 16 to 23 show the waveforms of the **two versions for leads I, II, and III, leads aVR, aVL and aVF, and leads V1 to V6. Cross-correlation coefficients of all the conventional 12 leads can be found in** [29].

We have the following observations during the experiments. (a) Synthesized 12-lead signals exhibit almost the same QRS complexes as those of the observed versions, except Lead V2. The high correlations during QRS-complex duration make the corresponding 9 cross-correlation coefficients higher than 0.75 (1 coefficient between 0.5 and 0.6, 2 coefficients below 5.5). (b) Two versions of signals show high degrees of similarity in the P-R segments, but large differences in S-T segments. (c) Synthesized 12-lead signals have amplified magnitudes, 1 to 4 times of those of the observed 12-lead signals.

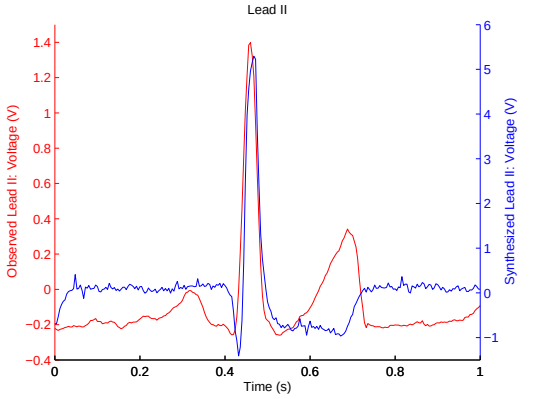

Fig. 15. Comparison between observed and synthesized Lead II signals.

B. Signal Reliability

During our practical testings of W3ECG, we have observed that movement of the subject, distance between the subject and the gateway, as well as the surrounding environment affect the quality of ECG signals.

Severe movements of the subject, such as running and jumping, have a direct influence on the average potential difference. A drift of the ECG signal or even a saturation can be observed. However, these movements have limited impact on ECG signals' transportation as long as the distance between the pads and gateway are well within 10 meters and line-of-sight links exist. We also noted that when the subject is walking away from the gateway, transportation quality degrades very abruptly when the distance reached 10 meters in an indoor environment or line-of-sight link is lost.

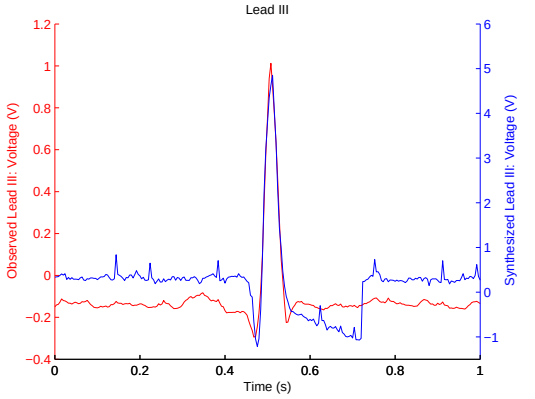

Fig. 16. Comparison between observed and synthesized Lead III signals.

VI. Conclusions

Complementing a number of existing ECG systems, we provide caregivers and patients another choice: W3ECG. With the goal of designing a wireless ECG system to render caregivers standard 12-lead ECG information, we have added

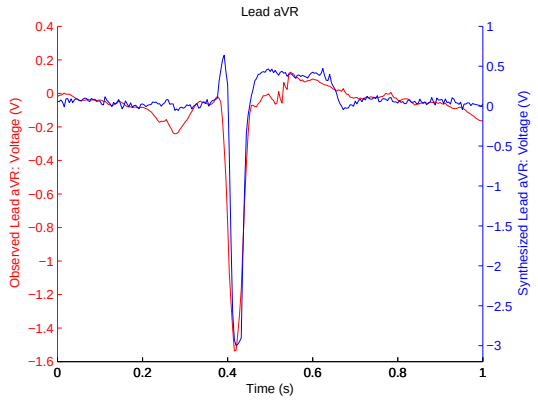

Fig. 17. Comparison between observed and synthesized Lead aVR signals.

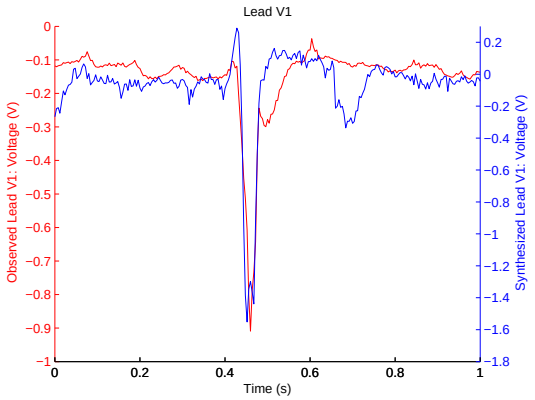

Fig. 20. Comparison between observed and synthesized Lead V1 signals.

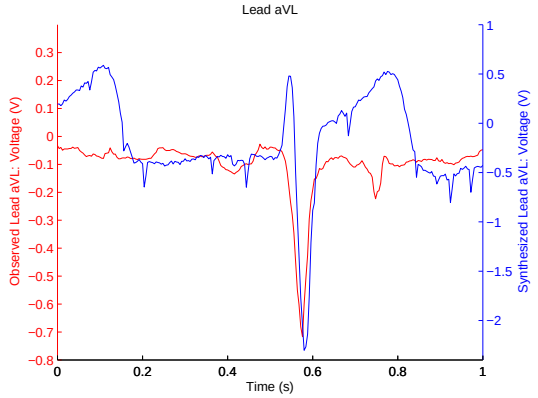

Fig. 18. Comparison between observed and synthesized Lead aVL signals.

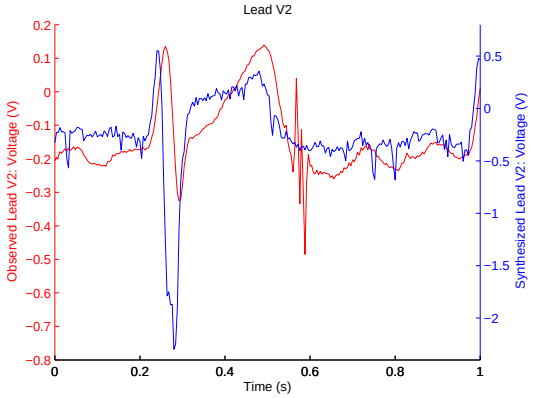

Fig. 21. Comparison between observed and synthesized Lead V2 signals.

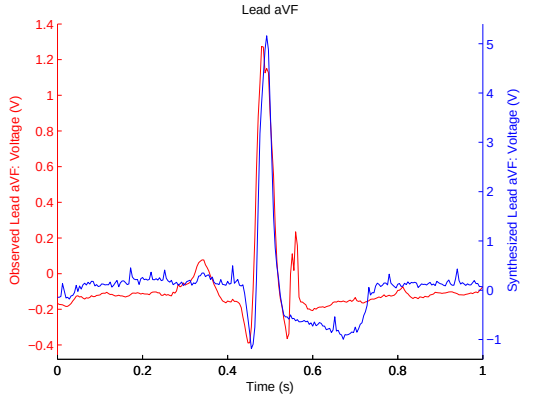

Fig. 19. Comparison between observed and synthesized Lead aVF signals.

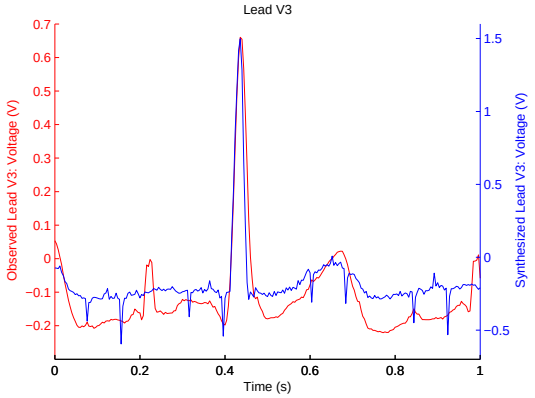

Fig. 22. Comparison between observed and synthesized Lead V3 signals.

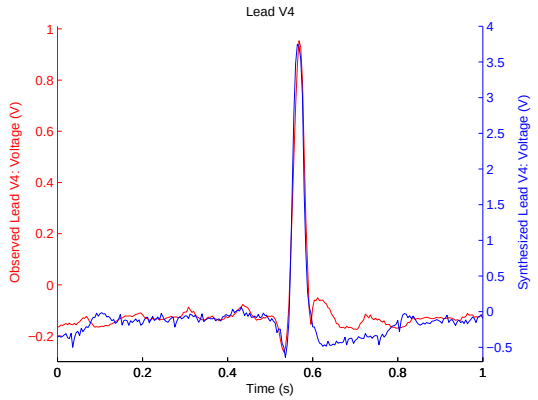

Fig. 23. Comparison between observed and synthesized Lead V4 signals.

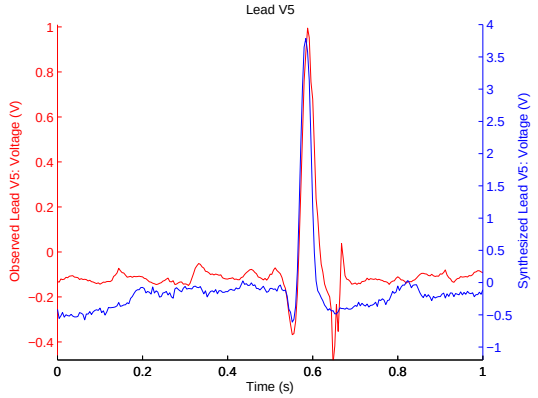

Fig. 24. Comparison between observed and synthesized Lead V5 signals.

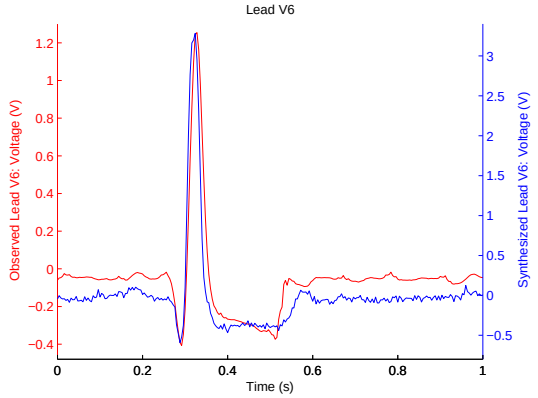

Fig. 25. Comparison between observed and synthesized Lead V6 signals.

another two pads to wireless single-pad ECG systems to gain spatial variety during recording. The criteria for evaluating pad placements have been discussed and one possible set of pad placements has been provided. Feasibility tests of our selected pad placement positions show comparable results with respect to the EASI lead system. Experiment studies also exhibit high correlations between synthesized and directly observed 12-lead signals (9 out of 12 cross-correlation coefficients higher than 0.75).

We intend to further our research on improving pad placements and evaluating our proposed system over a larger pool of patients. Our long term goal is to develop a wireless multiple-pad system that works in such a way that the placement of the pads is not critical. As aforementioned, the placements of pads are important, but not unique. Intelligence can be provided to facilitate the placement of pads in real-time by computing the corresponding transformation matrix.

ACKNOWLEDGMENT

The authors would like to thank Prof. Horacek from Dalhousie University, Canada, for providing clinical data and guidance required to conduct this study.

REFERENCES

[1] J. G. Webster, Ed., *Medical Instrumentation: Application and Design*, 3rd ed. Wiley, 1997.

[2] J. W. Hurst, "Naming of the waves in the ecg, with a brief account of their genesis," *Circulation Research*, vol. 98, pp. 1937 – 1942, 1998.

[3] R. Hoekema, G. J. H. Uijen, and A. van Oosterom, "On selecting a body surface mapping procedure," *Journal of Electrocardiology*, vol. 32, no. 2, pp. 93 – 101, 1999.

[4] D. D. Finlay, C. D. Nugent, J. G. Kellett, M. P. Donnelly, P. J. McCullagh, and N. D. Black, "Synthesising the 12-lead electrocardiogram: Trends and challenges," *European Journal of Internal Medicine*, vol. 18, no. 8, pp. 566 – 570, 2007.

[5] D. D. Finlay, C. D. Nugent, P. J. McCullagh, and N. D. Black, "Mining for diagnostic information in body surface potential maps: A comparison of feature selection techniques," *BioMedical Engineering OnLine*, vol. 4, 2005.

[6] B. Khaddoumi, H. Rix, O. Meste, M. Fereniec, and R. Maniewski, "Body surface ECG signal shape dispersion," *Biomedical Engineering, IEEE Transactions on*, vol. 53, pp. 2491 – 2500, 2006.

[7] B. M. Horacek, J. W. Warren, C. J. Penney, R. S. MacLeod, L. M. Title, M. J. Gardner, and C. L. Feldman, "Optimal electrocardiographic leads for detecting acute myocardial ischemia," *Journal of Electrocardiology*, vol. 34, pp. 97 – 111, 2001.

[8] G. E. Mailloux and R. M. Gulraajani, "Theoretical evaluation of the McFee and Frank vectorcardiographic lead systems using a numerical inhomogeneous torso model," *Biomedical Engineering, IEEE Transactions on*, vol. 29, pp. 322 – 332, 1982.

[9] B. M. Horacek, J. W. Warren, D. Q. Feild, and C. L. Feldman, "Statistical and deterministic approaches to designing transformations of electrocardiographic leads," *Journal of Electrocariology*, vol. 35, pp. 41 – 52, 2002.

[10] M. Munshi, X. Xu, X. Zou, E. Soetiono, C. S. Teo, and Y. Lian, "Wireless ECG plaster for body sensor network," in *Proceedings of the 5th International Workshop on Wearable and Implantable Body Sensor Networks (BSN 2008) in conjunction with the 5th International Summer School and Symposium on Medical Devices and Biosensors (ISSS-MDBS 2008)*, 2008.

[11] IMEC, http://www.imec.be/. [Online]. Available: http://www.imec.be/

[12] "Wireless medical diagnosis and monitoring equipment," U.S. Patent 6,577,893, 2003.

[13] E. Frank, "General theory of heart-vector projection," *Circulation Research*, vol. 2, pp. 258 – 270, 1954.

[14] C. Levkov, "Derived 12 channel electrocardiogram from 4 channel holter electrocardiogram," in *XI International Scientific and Applied Conference*, 2002.

[15] D. Q. Feild, C. L. Feldman, and B. M. Horacek, "Improved EASI coefficients: Their derivation, values, and performance," *Journal of Electrocardiology*, vol. 35, pp. 23 – 33, 2002.

[16] H. Cao, V. Leung, C. Chow, and H. Chan, "Enabling technologies for wireless body area networks: A survey and outlook," *IEEE Communications Magazine*, vol. 47, pp. 84 – 93, 2009.

[17] IEEE Computer Society, *802.15.4-2006 IEEE Standard for Information Technology- Telecommunications and Information Exchange Between Systems- Local and Metropolitan Area Networks- Specific Requirements Part 15.4: Wireless Medium Access Control (MAC) and Physical Layer (PHY) Specifications for Low-Rate Wireless Personal Area Networks (WPANs)*, Std.

[18] N. Golmie, D. Cypher, and O. Rebala, "Performance analysis of low rate wireless technologies for medical applications," *Comput. Commun.*, vol. 28, pp. 1266 – 1275, 2005.

[19] H. Cao, X. Liang, I. Balasingham, and V. Leung, "Performance analysis of zigbee technology for wireless body area sensor networks," in *Proceedings of The 2009 International Workshop on Advanced Sensor Integration Technology*, 2009.

[20] H. Cao, S. Gonzá́lez-Valenzuela, and V. Leung, "Employing ieee 802.15.4 for quality of service provisioning in wireless body area sensor networks," in *Proceedings of The IEEE 24th International Conference on Advanced Information Networking and Application*, 2010.

[21] A. Milenkovic, C. Otto, and E. Jovanov, "Wireless sensor networks for personal health monitoring: Issues and an implementation," *Comput. Commun.*, vol. 29, pp. 13 – 14, 2006.

[22] S. Yoo, D. Kim, M. Pham, Y. Doh, E. Choi, and J. Huh, "Scheduling support for guaranteed time services in ieee 802.15.4 low rate wpan," in *Proceedings of the 11th IEEE International Conference on Embedded and Real-Time Computing Systems and Applications, RTCSA05*, 2005.

[23] J. H. Hauer, "TKN15.4: An IEEE 802.15.4 MAC implementation for TinyOS 2," Technical University Berlin, Tech. Rep. TKN-08-003, 2009.

[24] A. Kopke and J. H. Hauer, "TKN15.4: An IEEE 802.15.4 symbol rate timer for TelosB," Technical University Berlin, Tech. Rep. TKN-08-006, 2008.

[25] K. Y. Yazdandoost and K. Sayrafian-Pour, "Channel model for body area network (BAN)," IEEE, Tech. Rep. IEEE P802.15-08-0780-08-0006, 2009.

[26] "PhysioNet/CinC Challenge 2007 Data Sets," http://www.physionet.org/challenge/2007/data/.

[27] Texas Instruments, http://www.ti.com/. [Online]. Available: http://www.ti.com/

[28] Moteiv Corporation. (2006) Tmote Sky: Quick Start Guide.

[29] H. Cao, H. Li, L. Stocco, and V. Leung, "Design and evaluation of a novel wireless three-pad ECG system for generating conventional 12-lead signals," in *Proceedings of The 5th International Conference on Body Area Networks*, 2010.

[30] CDC, "Centers for Disease Control and Prevention," http://www.cdc.gov/nchs/fastats/bodymeas.htm.

[31] TinyOS, http://www.tinyos.net/. [Online]. Available: http://www.tinyos.net/

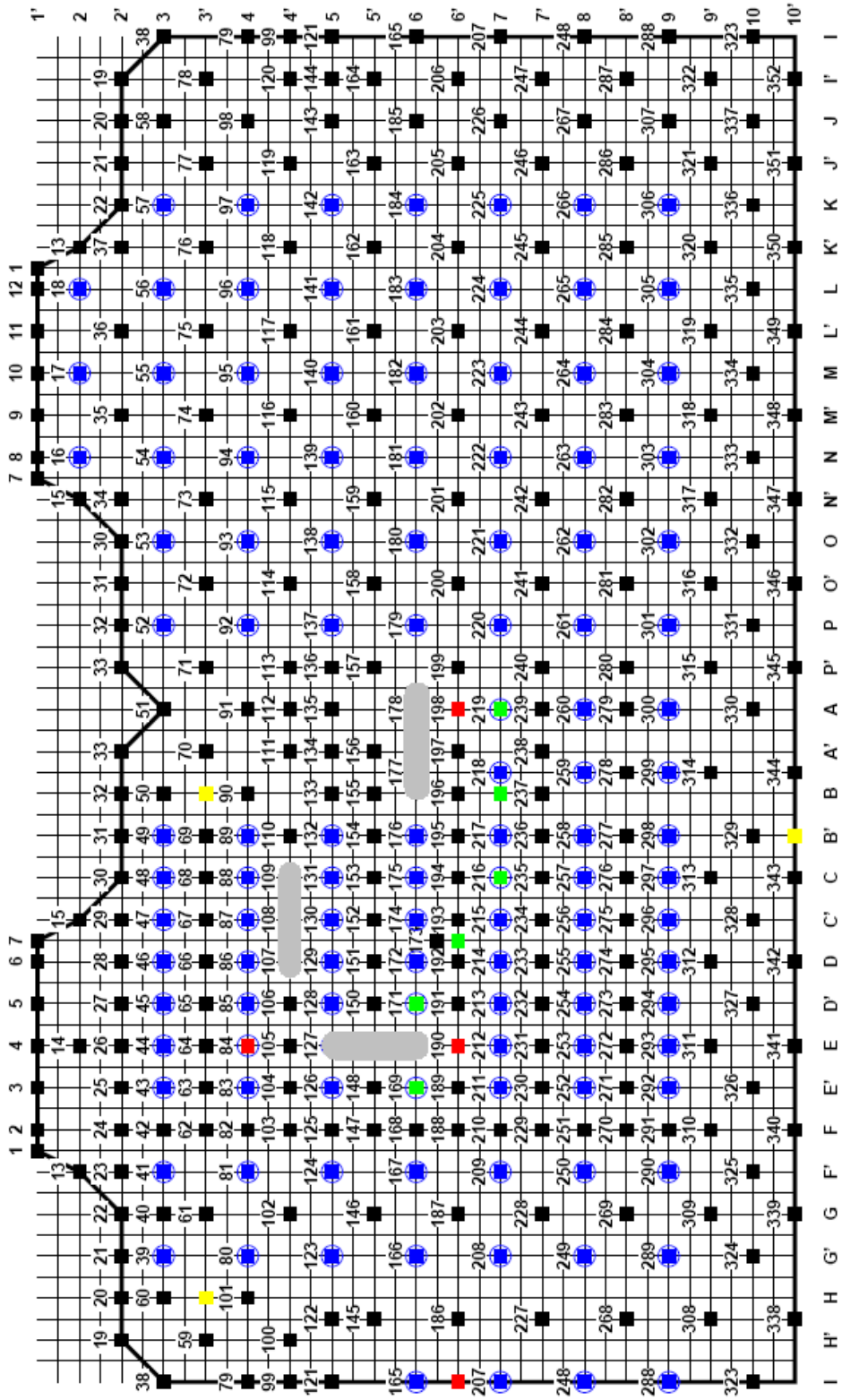

Fig. 1. Dalhousie's 2-D representation of human torso. (There are 352 numbered dots in the model. Circled dots represent measurement sites for Dalhousie's BSM system. Yellow dots represent electrode placement for RR, LR and LL, and green dots for V1 V6. Red dots represent electrode placement for EASI lead system. And greyed area represent pad placement for W3ECG system.)

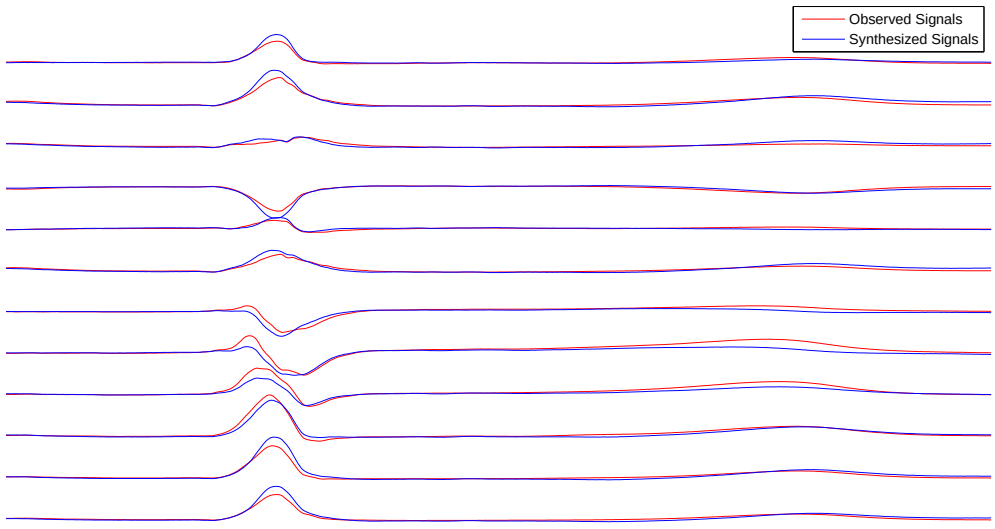

Fig. 9. Comparison between synthesized 12-lead ECG signals and directly obtained versions.

Fig. 12. A snapshot of W3ECG server GUI (Red, white and green traces represent synchronized ECG waveforms from Pad 1, Pad 2 and Pad 3, respectively).